Available online at www.sciencedirect.com
SCIENCE DIRECT®
Journal of Computational Physics 201 (2004) 191–203
JOURNAL OF COMPUTATIONAL PHYSICS
www.elsevier.com/locate/jcp

A mesoscopic simulation model for immiscible multiphase fluids

Yasuhiro Inoue [a,*], Yu Chen [b], Hirotada Ohashi [c]

[a] *Department of Mechanical Engineering, Graduate School of Engineering, University of Tokyo, 7-3-1 Hongo, Bunkyo-ku, Tokyo 113-8656, Japan*
[b] *Interfaculty Initiative in Information Studies, Graduate School of University of Tokyo, Tokyo, Japan*
[c] *Department of Quantum Engineering and Systems Science, Graduate School of Engineering, University of Tokyo, Tokyo, Japan*

Received 30 September 2003; received in revised form 15 March 2004; accepted 17 May 2004
Available online 25 June 2004

Abstract

We introduce a new scheme for real-coded lattice gas to the numerical simulation of immiscible multiphase fluids. This scheme is based on a minimization principle. A numerical example demonstrates the spontaneous segregation of N-phase in two dimensions. Numerical studies on the surface tension between two fluids show a good agreement with Laplace's law. The reproduction of Brownian motion for single droplet was verified through Maxwell–Boltzmann distribution of its velocity. A preliminary application illustrates a simulation of many immiscible droplets dispersed in another fluid.

PACS: 02.70.Ns; 47.11.+j; 82.20.Wt

Keywords: Multiphase fluid flows; Particle-based mesoscopic model; Real-coded lattice gas; Stochastic rotation dynamics

1. Introduction

Multiphase fluid flows occur widely in nature and engineering processes. Oil–water flows, boiling fluids, processing on paints, coatings and foodstuffs, biological fluids are cited. Since the effective interactions between solute–solute are modified by the fluid flows, the nature of the fluid is changed when an external flow field would be applied to the fluid. Therefore, a direct simulation of such a complex fluid is a challenging task. However, the dynamics of such systems occur on long-time scales and over long distances. Thus, the simulation model requires an ability to get access to both microscale and macroscale. One of

* Corresponding author. Tel.: +81-3-5841-6288; fax: +81-3-3943-9346.
E-mail address: inoue@fel.t.u-tokyo.ac.jp (Y. Inoue).

0021-9991/$ - see front matter
doi:10.1016/j.jcp.2004.05.008

candidates is a series of mesoscopic simulation models such as lattice Boltzmann method (LBM) [1,2], lattice gas automata (LGA) [3] and dissipative particle dynamics (DPD) [4].

Recently, a particle-based mesoscopic model for single-phase fluids was introduced by Malevanets and Kapral [5]. This model resembles LGA in synchronous discrete time evolution and in discretizing the space with regular lattices, but differs from LGA in using continuous velocities and multi particles in a single cell. Usually, a regular lattice with links of unit length is employed in [5], so that the cell is a square in 2D or a cube in 3D. The evolution of the system consists of two processes, namely, streaming and collision. The position of every particle is renewed in the streaming process and the update of velocity is done in the collision process. In this model, the mesoscopic dynamics preserve the conservation laws for mass, momentum and energy. As a result, the hydrodynamic equations are obtained in the macroscopic limit.

Malevanets and Kapral [5] employed a stochastic method for the complete translation of each particle in the simulation system. In particular, each particle is translated accurately only according to the integer part of its velocity. The fractional part of its velocity is used, however, as a probability distribution for a random walk process that followed. The consequence of this special translation is that particles can meet others at a lattice site (the crossing point of lattice links). Therefore, the "physical contacts" of particles are ensured in the pre-collision stage. However, the random walk process could be unnecessary for two reasons: first, collisions can occur among particles staying in a single cell instead of at a single site; second, since particles which have continuous positions are distributed uniformly within a single cell, translating particles accurately (according to both the integer and fractional part of coordinates) is equivalent to translating them from the randomly shifted locations (with integer coordinates). We realized these facts and modified the original model [5] to real-coded lattice gas (RLG) [6]. Note that Malevanets and Kapral [7] also developed the same idea independently at almost the same time. The computational efficiency of RLG is improved without the random walk process.

An analytical and numerical analysis on the fundamental questions such as the proof of Galilean invariance [8], the expression of transport coefficients [9–11] and the nature of thermal fluctuations of RLG [12] has been presented. Regarding RLG's major advantages, one may mention as follows: RLG has the simple algorithm, and the reproduction of thermal fluctuating hydrodynamics. The latter would be very useful, for example, in studying problems with flow instability or the Brownian motions. A variety of applications have already been studied using RLG method: the solvent dynamics [13], the dynamics of short polymer chains [14], the immiscible two-phase dynamics [6], the self-aggregation of amphiphilic surfactants [15] and the flow with solid suspensions [16]. With the encouraging results from these studies, it seems that RLG is very promising for the simulation of complex fluids.

The extension of [5] to the binary fluids was introduced by Hashimoto et al. [6], which we shall call immiscible real-coded lattice gas (IRLG), based on the two-component lattice gas model developed by Rothman and Keller [17]. Both dynamics of the phase segregation and dynamics of bubbles have been reproduced by IRLG. However, IRLG has no framework to simulate N-phase fluids. In this study, we present the new scheme for real-coded lattice gas to simulate immiscible multiphase fluids by introducing the N-color collision rule.

The outline of this paper is as follows. Section 2 outlines the single-phase RLG model. In Section 3, we describe the new extension that leads to multiphase fluids. Numerical simulations by our model are displayed in Section 4. The concluding remarks are given in Section 5.

2. Single-phase fluids model

First of all, it might be helpful to give an explanation of the single-phase RLG model. In the model, the particle dynamics consists of two processes, namely, streaming and collision. In the streaming, the position vector of each particle is shifted through a unit time interval as follows:

$$\mathbf{r}_i(t+1) = \mathbf{r}_i(t) + \mathbf{v}_i(t). \tag{1}$$

Here, $\mathbf{r}_i(t)$ and $\mathbf{v}_i(t)$ are the position and the velocity vectors of particle i at time t. In the collision, particles exchange their momentum and kinetic energy if they happen to reside in the same cell. The process is formulated as follows:

$$\mathbf{v}_i(t+1) = \mathbf{V}[\mathbf{r}_i(t)] + \mathbf{\Omega}(\mathbf{v}_i(t) - \mathbf{V}[\mathbf{r}_i(t)]) \quad . \tag{2}$$

Here, $\mathbf{V}[\mathbf{r}_i(t)]$ is the velocity of the center of mass for those "colliding particles". The vector in the bracket $[\mathbf{r}_i]$ stands for the integer part of $\mathbf{r}_i$. Taking the mass of particle i as m_i, $\mathbf{V}[\mathbf{r}_i(t)]$ can be calculated as

$$\mathbf{V}(\mathbf{R}_{lmn}, t) = \frac{1}{M(\mathbf{R}_{lmn}, t)} \sum_i m_i \mathbf{v}_i(t) \delta(\mathbf{R}_{lmn} - [\mathbf{r}_i(t)]) \ , \tag{3}$$

where $\mathbf{R}_{lmn} = l\mathbf{1}_x + m\mathbf{1}_y + n\mathbf{1}_z$ is the arbitrary lattice point vector which only has integer components. Unit vectors along the x-, y- and z-directions are indicated as $\mathbf{1}_x$, $\mathbf{1}_y$ and $\mathbf{1}_z$. The total mass in a cell can be calculated as follows:

$$M(\mathbf{R}_{lmn}, t) = \sum_i m_i \delta(\mathbf{R}_{lmn} - [\mathbf{r}_i(t)]) \ . \tag{4}$$

The collision matrix $\mathbf{\Omega}$ is usually selected randomly from a rotation group which can ensure the conservation of mass, momentum and energy. $\mathbf{\Omega}$ can be written explicitly, for example in 2D space with an arbitrary deflection θ as follows:

$$\mathbf{\Omega} = \begin{pmatrix} \cos\theta & -\sin\theta \\ \sin\theta & \cos\theta \end{pmatrix}. \tag{5}$$

The kinetic theory of such a particle dynamics proves both the Maxwell–Boltzmann type equilibrium and the existence of an H-theorem [7].

3. Multiphase fluids model

3.1. Introduction

In the immiscible binary model [6], the particles were colored either red or blue, and the collision rule was modified to obtain surface tension between the two fluids. This two-phase collision rule has been constructed from the intuitive belief on the phase-segregating behavior, and yet, extension of [6] to N-phase fluids may not appear straightforward. In this section, we introduce a multi-color collision rule in terms of a multi-color potential energy.

3.2. The definition of the color potential energy

We define the multi-color potential energy for a colored particle in the multi-color field. In the beginning, we define the color flux and the multi-color field for particle i. The color flux of particle i is a relative velocity against the colliding particles in a cell as follows:

$$\mathbf{p}_i = \mathbf{v}_i - \mathbf{V}[\mathbf{x}_i]). \tag{6}$$

The color field is a color gradient due to the color differences in neighboring cells as follows:

$$\mathbf{E}_i = \sum_{j;[\mathbf{x}_j]\neq[\mathbf{x}_i]} \frac{\kappa_{c_i c_j}}{|[\mathbf{x}_j]-[\mathbf{x}_i]|^d}([\mathbf{x}_j]-[\mathbf{x}_i])\delta(1-|[\mathbf{x}_j]-[\mathbf{x}_i]|). \tag{7}$$

Here, the reference to time t is omitted for the simplicity. c_i indicates the color of particle i, and the color takes one of blue, red, green, yellow and so on. $\kappa_{c_i c_j}$ indicates the amplitude parameter of the interaction between "c_i" color and "c_j" color. $\kappa_{c_i c_j}$ should take a positive real number for an attractive interaction or a negative real number for a repulsive interaction. d is the dimension number. In the above equation, we have taken only the nearest neighbor sites.

To couple the multi-color interaction with the particle collision process equation (2), we define the color torque $\mathbf{N}_i$ of particle i as follows:

$$\mathbf{N}_i \equiv (\mathbf{v}_i - \mathbf{V})\times \mathbf{E}_i, \tag{8}$$

$$= \mathbf{p}_i \times \mathbf{E}_i, \tag{9}$$

$$= p_i E_i \sin(\phi_i)\hat{\phi}_i. \tag{10}$$

Here, ϕ_i indicates the angle from $\mathbf{E}_i$ to $\mathbf{p}_i$ on the plane $p_i E_i$ which consists of $\mathbf{E}_i$ and $\mathbf{p}_i$. $\hat{\phi}_i$ is the unit vector normal to the plane $p_i E_i$. We take the plus direction of $\hat{\phi}_i$ for the increment of ϕ_i.

Now, we consider the torque work. The torque work $\mathrm{d}W_i$ of the infinitesimal rotation by the angle $\mathrm{d}\phi$ is calculated as the following:

$$\mathrm{d}W_i = \mathbf{N}_i \cdot \mathrm{d}\phi\hat{\phi}_i = p_i E_i \sin(\phi_i)\,\mathrm{d}\phi. \tag{11}$$

Thus, the whole work from ϕ_i to ϕ_i' is the following:

$$\int_{\phi_i}^{\phi_i'} \mathrm{d}W_i = p_i E_i \cos(\phi_i') - p_i E_i \cos(\phi_i). \tag{12}$$

The multi-color potential energy U_i of particle i is defined as the work against $\mathrm{d}W_i$ along the opposite path

$$U_i = \int_{\phi_i'}^{\phi_i} -\mathrm{d}W_i, \tag{13}$$

$$= -p_i E_i \cos(\phi_i), \tag{14}$$

$$= -\mathbf{p}_i \cdot \mathbf{E}_i. \tag{15}$$

Here, we choose $\phi_i' = \pi/2$ as the potential origin. From Eq. (15), it is clear that U_i is the minimum value when $\mathbf{p}_i$ is parallel to $\mathbf{E}_i$.

3.3. The algorithm for multiphase fluids

In this section, we describe the kernel algorithm of multiphase fluids. The algorithm is based on the minimization of the multi-color potential energy with the time evolution, and the algorithm is implemented in the multi-particle collision Eq. (2). Since the multi-particle collision is operated at each cell, we shall define the multi-color potential energy at each cell. Thus, we take the sum of the multi-color potential energy over all particles as follows:

$$\sum_i U_i = \int \mathrm{d}V \sum_c U_c(\mathbf{X}). \tag{16}$$

Here, c indicates the color such as blue, red, yellow, and so on, and

$$U_c(\mathbf{X}) = \sum_i U_i \delta_{cc_i} \delta(\mathbf{X} - [\mathbf{x}_i]), \tag{17}$$

$$= -\mathbf{q}_c(\mathbf{X}) \cdot \mathbf{F}_c(\mathbf{X}), \tag{18}$$

$$\mathbf{q}_c(\mathbf{X}) = \sum_i \mathbf{p}_i \delta_{cc_i} \delta(\mathbf{X} - [\mathbf{x}_i]), \tag{19}$$

$$\mathbf{F}_c(\mathbf{X}) = \sum_{j;[\mathbf{x}_j] \neq \mathbf{X}} \frac{\kappa_{cc_j}}{|[\mathbf{x}_j] - \mathbf{X}|^d} [\mathbf{x}_j] - \mathbf{X}) \delta(1 - |[\mathbf{x}_j] - \mathbf{X}|). \tag{20}$$

Thus, the local multi-color potential energy is defined from Eq. (16) as

$$U(\mathbf{X}) = \sum_c U_c(\mathbf{X}). \tag{21}$$

To reduce $U(\mathbf{X})$ with the time evolution, all the color flux in the same cell should be rotated simultaneously in the collision process equation (2) by an adaptive angle where $U(\mathbf{X})$ is a minimum. Therefore, we derive the adaptive angle in the next.

After the multi-particle collision, the color flux of particle i would be changed as

$$\mathbf{p}_i(t+1) = \mathbf{\Omega}\mathbf{p}_i(t). \tag{22}$$

Here, t indicates the reference to time. Thus, $U(\mathbf{X}, t+1)$ is calculated as

$$U(\mathbf{X}, t+1) = \cos(\theta) \sum_c \mathbf{q}_c(\mathbf{X}, t) \cdot \mathbf{F}_c(\mathbf{X}, t) - \sin(\theta)\hat{\mathbf{z}} \cdot \sum_c \mathbf{q}_c(\mathbf{X}, t) \times \mathbf{F}_c(\mathbf{X}, t), \tag{23}$$

and we can see that $U(\mathbf{X}, t+1)$ vary with θ of the collision matrix $\mathbf{\Omega}$. Differentiating $U(\mathbf{X}, t+1)$ with respect to the angle θ, we obtain

$$\frac{\partial U(\mathbf{X}, t+1)}{\partial \theta} = \sin(\theta) \sum_c \mathbf{q}_c(\mathbf{X}, t) \cdot \mathbf{F}_c(\mathbf{X}, t) - \cos(\theta)\hat{\mathbf{z}} \cdot \sum_c \mathbf{q}_c(\mathbf{X}, t) \times \mathbf{F}_c(\mathbf{X}, t). \tag{24}$$

We define θ_0 and θ_0^* as extremal values of Eq. (24) with the condition $\partial U/\partial\theta = 0$. These angles satisfy the following equations:

$$\tan(\theta_0) = \frac{\hat{\mathbf{z}} \cdot \sum_c \mathbf{q}_c(\mathbf{X}, t) \times \mathbf{F}_c(\mathbf{X}, t)}{\sum_c \mathbf{q}_c(\mathbf{X}, t) \cdot \mathbf{F}_c(\mathbf{X}, t)}, \tag{25}$$

$$\theta_0^* = \theta_0 + \pi. \tag{26}$$

To find out an adaptive angle, we investigate the gradient of $U(\mathbf{X}, t+1)$ at the neighborhood around these extremal values. In the advance, we rewrite some functions to the simple one as follows:

$$g(\theta) = \left.\frac{\partial U(\mathbf{X}, t+1)}{\partial \theta'}\right|_{\theta'=\theta}, \tag{27}$$

$$U = \sum_c \mathbf{q}_c(\mathbf{X}, t) \cdot \mathbf{F}_c(\mathbf{X}, t), \tag{28}$$

$$N = \hat{\mathbf{z}} \cdot \sum_c \mathbf{q}_c(\mathbf{X}, t) \times \mathbf{F}_c(\mathbf{X}, t). \tag{29}$$

At $\theta = \theta_0 + \Delta\theta$

$$g(\theta_0 + \Delta\theta) = U\sin(\theta_0 + \Delta\theta) - N\cos(\theta_0 + \Delta\theta), \tag{30}$$

$$= U\frac{\sin(\Delta\theta)}{\cos(\theta_0)}, \tag{31}$$

$$\sim \frac{U\Delta\theta}{\cos(\theta_0)}. \tag{32}$$

To derive Eq. (32) from Eq. (31), we use Taylor expansions and neglect the higher order terms. Table 1 shows the sign of the numerator of $g(\theta)$ around θ_0. Thus, we can conclude that the adaptive angle θ_a should be as follows:

$$\theta_a = \begin{cases} \theta_0 & \text{if } U > 0, \\ \theta_0^* & \text{if } U < 0. \end{cases} \tag{33}$$

The kernel algorithm of the multiphase fluids model is briefly summarized as a three-step update. First, the color flux and field are calculated by Eqs. (6) and (7) for each particle in the same cell. Second, candidates of the adaptive angle θ_a are calculated by Eqs. (25) and (26), and then θ_a is determined by the condition (33). Lastly, particles obey the multi-particle collision Eq. (2) by the rotation angle $\theta = \theta_a$.

3.4. Comparison with the former IRLG

Turning now to the relation between IRLG [6] and our present model, the former model is regarded as the limited case in our model. To show this, we choose the amplitude parameter $\kappa_{c_i c_j}$ as the following:

$$\kappa_{c_i c_j} = \begin{cases} +1, & c_i = c_j, \\ -1, & c_i \neq c_j. \end{cases} \tag{34}$$

Here, c_i indicates the color of ith particle. The color takes either red or blue, because IRLG is a binary model. In this case, we can derive the following relation from Eq. (20):

$$\mathbf{F}_r = -\mathbf{F}_b. \tag{35}$$

Here, subscript r/b indicate red/blue. Substituting the above relation into Eq. (21), we can calculate the local color potential energy U as follows:

$$U = -\mathbf{q}_r \cdot \mathbf{F}_r - \mathbf{q}_b \cdot \mathbf{F}_b \tag{36}$$

$$= -\mathbf{q} \cdot \mathbf{F}_r. \tag{37}$$

Here, $\mathbf{q} \left(= \mathbf{q}_r - \mathbf{q}_b\right)$. From Eq. (37), we can find that the local color potential energy is the inner product of the net flux $\mathbf{q}$ and the field $\mathbf{F}_r$. The minimum energy state may then be determined where $\mathbf{q}$ is parallel to $\mathbf{F}_r$. The corresponding collision matrix $\mathbf{\Omega}$ is the following:

Table 1
The sign of the numerator of $g(\theta)$

	$\theta_0 - \Delta\theta$	θ_0	$\theta_0 + \Delta\theta$
$U > 0$	−	0	+
$U < 0$	+	0	−

$$\mathbf{\Omega} = \begin{pmatrix} \tilde{q}_x\tilde{f}_x + \tilde{q}_y\tilde{f}_y & -\tilde{q}_x\tilde{f}_y + \tilde{q}_y\tilde{f}_x \\ \tilde{q}_x\tilde{f}_y - \tilde{q}_y\tilde{f}_x & \tilde{q}_x\tilde{f}_x + \tilde{q}_y\tilde{f}_y \end{pmatrix}. \tag{38}$$

Here, $\tilde{\mathbf{q}} = \mathbf{q}/|\mathbf{q}|$ and $\tilde{\mathbf{f}} = \mathbf{F}_r/|\mathbf{F}_r|$. The collision matrix (38) is the same as one in the former IRLG model.

Clearly, the condition (34) leads our model to the former IRLG model. To put it another way, we can simulate flows of a binary fluid with other conditions on $\kappa_{c_ic_j}$ by using the present model. Furthermore, the present model is able to be applied to multi-component fluids as showing in the following section, while the former model can not.

4. Numerical simulations

4.1. Introduction

RLG simulations on a droplet have been carried out by using the former IRLG model [6]: the Galilean invariance of the motion of a droplet is verified through the comparison under static and uniform flow conditions [19]. The steady-state shape of a rising bubble for various the Etövös number E_o and the Morton number M is investigated [19–21], and the diagram of the steady-state shape as a function of E_o and M is agreed with [22]. In [23], the deformation of 2D single droplet in a linear shear flow as a function of capillary number is agreed with 2D lattice Boltzmann simulation of [24]. With results from these studies, it seems that IRLG, as well as the binary limit of the present model, are good agreement with conventional studies.

Now, we carried out other numerical simulations to show the effectiveness of our model.

The first simulation is for a phase segregation. In this simulation, we verified the multi-color collision rule equation (33) by reproducing a phase segregating behavior. Our present model could simulate a phase segregation of five fluids, while the former IRLG model could not treat multi-component fluids consist over two species.

In the second simulation, we confirmed Laplace's law on the surface tension. Laplace's law is satisfied in the present model.

The third is the simulation of Brownian motion of a droplet. The droplet was driven by the thermal fluctuation of the solvent. We confirmed that the probability distribution for the velocity of single droplet agreed with Maxwell–Boltzmann distribution.

The last is a simulation of many immiscible droplets. Many immiscible droplets are regarded as vesicles suspended in another fluid, which is so-called emulsion. A vesicle is a closed thin membrane separating the internal fluid from the external solvent, and this is the fundamental structure of a red blood cell. Blood consists of two parts. One is the solvent fluid called plasma, and the other is cells. Red blood cell (RBC) is the most dominant cell on blood flows, because its volume fraction is typically 40% of blood. Considering blood flows from the heart to capillary vessels, blood flows might be roughly decided into three categories owing to the comparison between the size of a RBC and the diameter of blood vessels.

(1) *Artery*: Blood may be regarded as a homogeneous visco-elastic fluid, because the diameter of blood vessels is enough larger than the size of a RBC. Casson model would be the most famous one [18].
(2) *Arteriole*: The assumption of homogeneity for blood has been broken down, because the diameter of blood vessels may be of the order of the size of a RBC. Blood should be modeled explicitly as RBC and fluid.
(3) *Capillary*: A precise mechanical modeling on the membrane of a RBC should be required, because the diameter of blood vessels is comparable with the size of a RBC or smaller.

We want the last simulation to open the way to simulate blood flows in (2) mentioned above, because the aggregation of RBCs and its volume are the main topics in this scale due to the high volume fraction of RBCs, where a precise modeling of a RBC is of less importance unless we would focus on flows in capillary vessels.

The numerical conditions of each simulation are as follows. The mean number density of particles was set to 20. Particles' momenta were initialized by using the Maxwell–Boltzmann distribution with a temperature T. The mean flow velocity was kept as zero. The mass of each particle was 1.

4.2. Phase segregation

Fig. 1 shows the simulation of a five-fluid phase segregation using the immiscible multiphase fluids model mentioned above. The calculations were carried out in a 2D system of the size 128×128 cells with doubly periodic boundary conditions. Particles' initial positions are decided in random. The volume fraction of each species is the same. The interaction parameter $\kappa_{c_ic_j}$ is chosen as follows, thus all of the surface tension coefficients is equal to each other

$$\kappa_{cc'} = \begin{cases} 1 & \text{when } c = c', \\ -1 & \text{when } c \neq c'. \end{cases} \tag{39}$$

Here, c and c' indicate an arbitrary color.

In Fig. 1, we can observe that five colored fluids are separated to a quasi hexagonal configuration with the time evolution, and each fluid makes an angle of $2\pi/3$ with respect to other two fluids in an equilibrium state at 60,000 time steps.

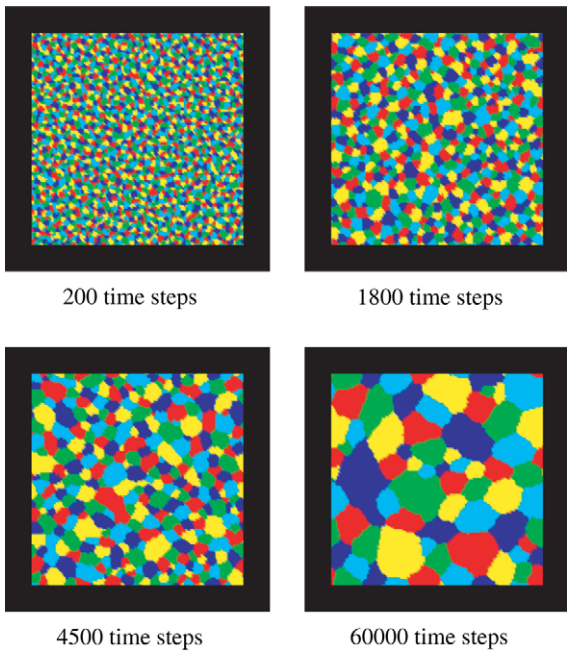

Fig. 1. Nonequilibrium behavior of a five-fluid phase segregation with equal surface tensions in 128×128 cells. The initial configuration is a random mixture.

4.3. Laplace's law

We test our model against Laplace's law in two dimensions

$$\Delta P = P_{\text{in}} - P_{\text{out}} = \frac{\sigma}{R}. \tag{40}$$

Here, in/out indicate "inner/outer" pressure of a 2D droplet of radius R. σ indicates the surface tension coefficient of a 2D droplet. Measurements of ΔP were started after 2000 time steps lasting for 2000 time steps in a system of the size $4R \times 4R$, and the calculation was performed five times with different initial configurations. The temperature of a system is ranging from 0.1 to 2.0. Fig. 2 shows that surface tension measured in our model obeys Laplace's law.

4.4. Brownian motion of a droplet

We test the Brownian motion of the single droplet of the radius of 8 cells suspended in the fluctuating fluid. The calculation was carried out in 2D system of the size 128×128. The background fluid is statistically isotropic and stationary, namely, the mean flow velocity is zero. The temperature of the system was set to 0.1. The velocity of the center of mass of the droplet was recorded for 2000000 times step, and then we calculated the probability distribution function (PDF) for the velocity of the droplet. In the thermal equilibrium state, the PDF should be Maxwell–Boltzmann distribution with the temperature of the system.

The calculated PDF is shown in Fig. 3. We fit the numerical data with Maxwell–Boltzmann distribution via the temperature T and the mean velocity v_0 as follows:

$$n(v) = \sqrt{\frac{M}{2\pi T}} \exp\left(-\frac{M(v - v_0)^2}{2T} \right) \Delta v. \tag{41}$$

Here, v indicates the velocity of the center of mass of the droplet, M is the total mass of the droplet and Δv indicates the interval between v and $v + \Delta v$. In the calculation of PDF, Δv was set to 10^{-4} and the velocity between v and $v + \Delta v$ was regarded as v.

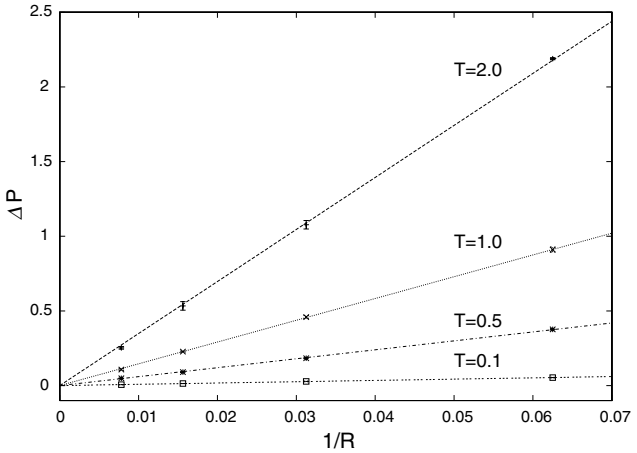

Fig. 2. Numerical verification of Laplace's law on our model. ΔP indicates the pressure difference between the inner and the outer pressure of a droplet. R is the radius of a droplet.

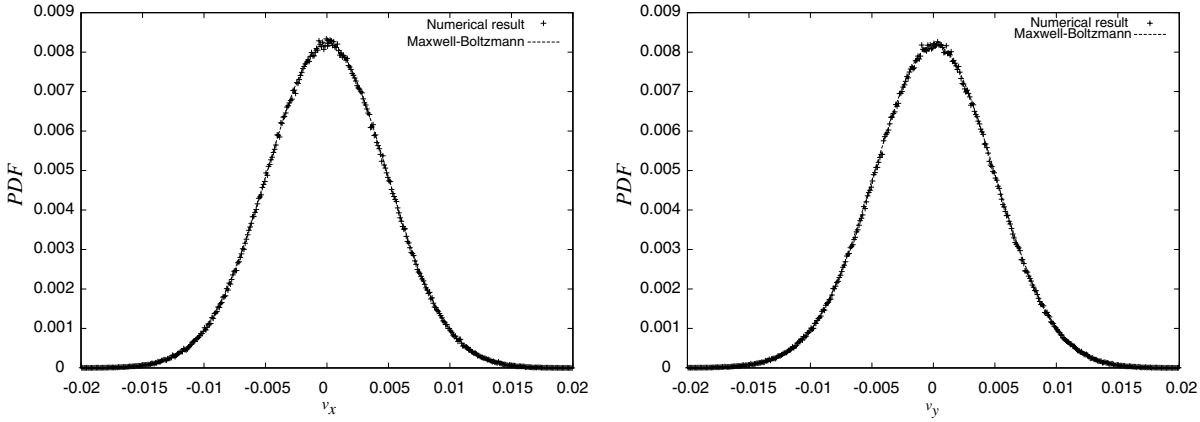

Fig. 3. Probability distribution function (PDF) for the velocity of the single droplet. The cross (+) indicates numerical results. The doted line indicates Maxwell–Boltzmann distribution with the temperature T and the mean velocity v_0.

Table 2
The value of fitting parameters of Eq. (41)

	T	v_0
x	9.7×10^{-3}	-1×10^{-6}
y	9.8×10^{-3}	8.3×10^{-5}

The fitting parameters are shown in Table 2. Table 2 shows that T is the same as the temperature of the system and v_0 is zero within the size of Δv, namely, the PDF for the velocity of the droplet is agreed with Maxwell–Boltzmann distribution as expected. This means that the droplet was doing the Brownian motion driven by the thermal fluctuation of background fluid.

4.5. Immiscible droplets

Two simulations of immiscible droplets suspended in another fluid were carried out in this section. The interaction parameters are displayed in Table 3. In both cases, the initial configuration of droplets is a regular lattice. The equilibrium shape of each droplet is a circle with the radius of 4 cells. The total number of droplets is 121, namely, the total number of species is 122 included one-solvent fluid. The temperature T of the system is set to 0.1 so that the droplet motion can be driven by thermal fluctuations in the solvent.

The simulation results in the first case are displayed in Fig. 4. In this case, the interaction parameter was chosen to set

Table 3
The interaction parameter

	κ_{vv}	κ_{sv}	κ_{ss}	$\kappa_{ss'}$
Case 1	1.0	−1.0	3.0	−30.0
Case 2	1.0	−1.0	3.0	−5.0

Subscript v indicates the color of solvent, s indicates the color of a droplet and s′ indicates the color of other droplets.

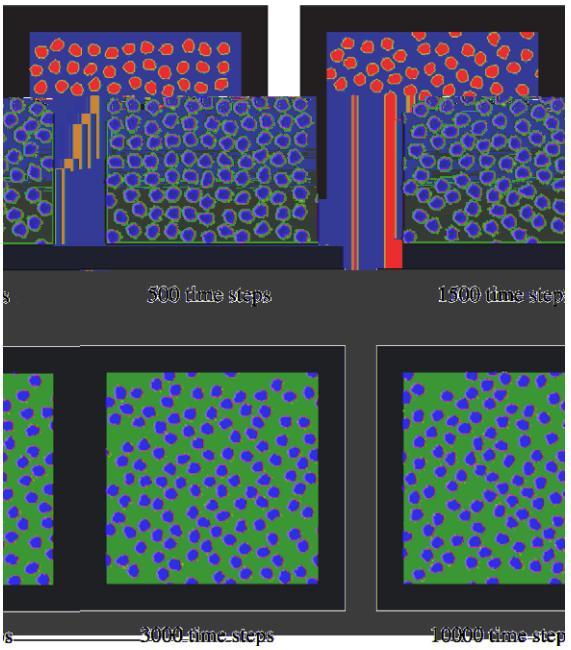

Fig. 4. Droplets are separated by the solvent due to $\sigma_{ss'} > 2\sigma_{sv}$, and the random configuration of droplets results from Brownian motion driven by the thermal fluctuations of the solvent.

$$\sigma_{ss'} > 2\sigma_{sv}. \tag{42}$$

Here, $\sigma_{ss'}$ indicates the surface tension coefficient between two droplets and σ_{sv} indicates the surface tension coefficient between a droplet and the background solvent. When the simulation started, these droplets were naturally driven by solvent particles and began to do the Brownian motion. Since $2\sigma_{sv}$ is less than $\sigma_{ss'}$, the triple contact points of droplet–droplet–solvent are not stable. Thus, the dispersion of droplets is in equilibrium when droplets are separated by the solvent. This is so-called the stable colloid dispersion.

The simulation results in the second case are displayed in Fig. 5. The interaction parameter was chosen to set

$$\sigma_{ss'} < 2\sigma_{sv}, \tag{43}$$

so that the triple contact points are stable. Thus, droplets could form aggregates, but not coalesce due to the immiscible multiphase algorithm. Furthermore, aggregates developed bigger forms with the time evolution. The resulting system is so-called the unstable colloid dispersion.

The way of modeling emulsion as many droplets is also appeared in a many-bubble model of the immiscible lattice gas cellular-automata by Rothman and Zaleski [25]. Our simulation result is found to be a qualitative agreement with the result in [25], even though our algorithm is different from their model.

Rothman and Zaleski have developed three-component immiscible LGA model based on their binary model, and then they applied three-component model to the simulation of many-bubble suspended in another. In their approach, the collision of colored particle is decided by minimizing the color potential energy for only two or three dominant components while the other has been neglected. This is the difference on the treatment of N-collision between [25] and our model. This simplification of multi-color collision may be reasonable only when the concentration of colors would not be high. In fact, N-collision would happen

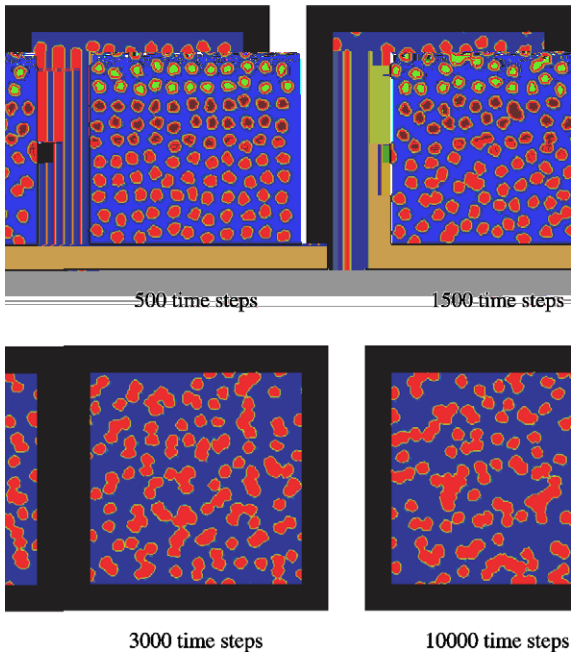

Fig. 5. Droplets can form aggregates due to $\sigma_{ss'} < \sigma_{sv}$, and aggregates grow bigger with the time evolution.

rarely if the system would be initialized as N-bubble, so that each model seems to be of consistent qualitatively.

5. Conclusions

We have developed a new scheme for the simulation of immiscible multiphase fluids. The RLG model is shown to have a huge potential for the simulation of complex flows. Our model is able to deal with N-fluid interactions that leads to the N-phase segregation. Brownian motions of immiscible droplets are naturally reproduced in the simulation and the stability of dispersion of immiscible droplets can be controlled by the interaction parameter $\kappa_{cc'}$. In the near future, we will verify the quantitative accuracy of this model through benchmarks on the dynamics of an immiscible many-droplet in 3D.

References

[1] G.R. Mcnamara, G. Zanetti, Use of the Boltzmann equation to simulate lattice-gas automata, Phys. Rev. Lett. 61 (1988) 2332.
[2] S. Chen, G.D. Doolen, Lattice Boltzmann method for fluid flows, Ann. Rev. Fluid Mech. 30 (1998) 329.
[3] U. Frisch, B. Hasslacher, Y. Pomeau, Lattice-gas automata for the Navier–Stokes equations, Phys. Rev. Lett. 56 (1986) 1505.
[4] P.J. Hoogerbrugge, J.M.V.A. Koelman, Simulating microscopic hydrodynamics with dissipative particle dynamics, Europhys. Lett. 19 (1992) 155.
[5] A. Malevanets, R. Kapral, Continuous-velocity lattice-gas model for fluid flow, Europhys. Lett. 44 (5) (1998) 552.
[6] Y. Hashimoto, Y. Chen, H. Ohashi, Immiscible real-coded lattice gas, Comput. Phys. Commun. 129 (2000) 56.
[7] A. Malevanets, R. Kapral, Mesoscopic model for solvent dynamics, J. Chem. Phys. 10 (1999) 8605.
[8] T. Ihle, D.M. Kroll, Stochastic rotation dynamics. I. Formalism, Galilean invariance, and Green–Kubo relations, Phys. Rev. E 67 (2003) 066705.

[9] T. Ihle, D.M. Kroll, Stochastic rotation dynamics. II. Transport coefficients, numerics, and long-time tails, Phys. Rev. E 67 (2003) 066706.
[10] N. Kikuchi, C.M. Pooley, J.F. Ryder, J.M. Yeomans, Transport coefficients of a mesoscopic fluid dynamics model, J. Chem. Phys. 119 (12) (2003) 6388.
[11] E. Tuzel, M. Strauss, T. Ihle, D.M. Kroll, Transport coefficients for stochastic rotation dynamics in three dimensions, Phys. Rev. E 68 (2003) 036701.
[12] Y. Inoue, Y. Chen, H. Ohashi, On the density correlation of the spontaneous fluctuation in a real-coded lattice gas, Comput. Phys. Commun. 153 (2003) 66.
[13] A. Malevanets, R. Kapral, Solute molecular dynamics in a mesoscale solvent, J. Chem. Phys. 112 (2000) 7260.
[14] A. Malevanets, J.M. Yeomans, Dynamics of short polymer chains in solution, Europhys. Lett. 52 (2000) 231.
[15] T. Sakai, Y. Chen, H. Ohashi, Real-coded lattice gas model for ternary amphiphilic fluids, Phys. Rev. E 65 (2002) 031503.
[16] Y. Inoue, Y. Chen, H. Ohashi, Development of a simulation model for solid objects suspended in a fluctuating fluid, J. Stat. Phys. 107 (2002) 85.
[17] D.H. Rothman, J. Keller, Immiscible cellular-automaton fluids, J. Stat. Phys. 52 (1988) 1119.
[18] Y.C. Fung, Biomechanics: Mechanical Properties of Living Tissues, second ed., Springer, New York, 1993.
[19] Y. Hashimoto, 'A numerical study of multi-phase flows using immiscible real-coded lattice gas model', Doctor Thesis, University of Tokyo, 1999.
[20] Y. Hashimoto, S. Teng, Y. Chen, H. Ohashi, Simulation of single bubble behavior using multi-component RLG, in: 9th International Conference on Discrete Simulation of Fluid Dynamics, 2000.
[21] Y. Kobayashi, 'Motion of a single bubble in real-coded lattice gas', Master Thesis, University of Tokyo, 2000.
[22] R. Clift, J.R. Grace, M.E. Weber, Bubbles, Drops, and Particles, Academic Press, New York, 1978.
[23] Y. Inoue, S. Takagi, Y. Matsumoto, A preliminary study on flows of vesicle suspension in the micro-circulation by using real-coded lattice gas, in: Proceedings of 17th Symposium on Computational Fluid Dynamics (Japanese), vol. 17, 2003, p. 223.
[24] N. Takada, Numerical simulation of two-phase flow using Lattice–Boltzmann method, Web J. Japan Soc. Fluid Mech. 11 (3) (2003) 98.
[25] D.H. Rothman, S. Zaleski, Lattice-Gas Cellular Automata: Simple Models of Complex Hydrodynamics, Cambridge University Press, Cambridge, 1997.